

$^{78,80,82}\text{Kr}(d,p)^{79,81,83}\text{Kr}$ reactions*

J. Chao, D. K. Olsen, † C. Newsom, and P. J. Riley

Center for Nuclear Studies, The University of Texas, Austin, Texas 78712

(Received 26 August 1974)

The level structures of $^{79,81,83}\text{Kr}$ have been investigated via the (d,p) stripping reaction using isotopically enriched gas targets at an incident deuteron energy of 11 MeV. Proton groups leading to about 14 states with excitation energies up to approximately 3 MeV have been identified in each of the above nuclei. Differential cross sections were measured from 20° to 160° , and were fitted with zero-range distorted-wave-Born-approximation calculations. Excitation energies, l values, spectroscopic factors, and the implied values of J^π are given. Comparisons are made with states in the selenium and germanium isotopes having the same number of neutrons and, respectively, one and two protons less than the krypton isotopes. Comparisons are also made between the present work and studies of ^{79}Kr via ^{79}Rb decay measurements. Two unresolved discrepancies are found between the two sets of measurements.

[NUCLEAR REACTIONS $^{78,80,82}\text{Kr}(d,p)^{79,81,83}\text{Kr}$, $E=11.0$ MeV, measured $\sigma(\theta)$]
and level energies; deduced l , S with DWBA analysis.

I. INTRODUCTION

The (d,p) reaction has been widely used to give information about the emptiness of spherical single-particle states in the target nucleus. For nuclei with an odd number of neutrons between the $N=28$ and $N=50$ shell closures systematic investigations have been made for nickel,¹ zirconium,² germanium,³ and selenium.⁴ In this paper we report on a systematic study of the lighter krypton isotopes.⁵ Cross section measurements for the $^{84}\text{Kr}(d,p)$ and $^{86}\text{Kr}(d,p)$ reactions have been previously reported.^{6,7} In the present work, (d,p) measurements were made using enriched gaseous targets of ^{78}Kr , ^{80}Kr , and ^{82}Kr , at a deuteron bombarding energy of 11.0 MeV. Proton groups leading to approximately 14 states in each of the final nuclei ^{79}Kr , ^{81}Kr , and ^{83}Kr have been identified. Many of these states have not been previously reported, owing to the scarcity of work on these isotopes. The ^{86}Kr nucleus has a closed $N=50$ neutron shell; ^{78}Kr , the lightest stable isotope of krypton, has 42 neutrons. The present measurements should therefore allow rather accurate measurements of the filling of the $2p_{3/2}$, $2p_{1/2}$, and $1g_{9/2}$ subshells lying below the $N=50$ shell closure as the neutron number is increased from 42 to 50. Comparisons with the previous (d,p) measurements on $^{76,78,80}\text{Se}$, with 42, 44, and 46 neutrons, respectively, and ^{74}Ge , ^{76}Ge , with 42 and 44 neutrons, should be of interest. The levels of ^{79}Kr have been studied via ^{79}Rb decay measurements by Lingeman *et al.*⁸ and by Broda *et al.*⁹ A comparison of the $^{78}\text{Kr}(d,p)^{79}\text{Kr}$ works with the level structure deduced from these

γ -decay measurements should therefore be possible.

II. EXPERIMENTAL PROCEDURE

Differential cross sections of the $\text{Kr}(d,p)\text{Kr}$ reactions and of deuteron elastic scattering were measured from 20° to 160° in 5° steps at a bombarding energy of 11.0 MeV. The target gases were contained in a 7.5-cm-diam cylindrical cell whose walls were of 3- μm Mylar foil. Nickel windows of 0.5- μm thickness were used for the beam entrance and exit. The gas cell utilized a thin-walled beam tube of 5.0-mm i.d. inside the target cell. A 1.27-cm gap in this tube at the center of the chamber defined the target volume. The gas pressure was approximately 0.025 atm corresponding to a target thickness of about 80 $\mu\text{g}/\text{cm}^2$. The respective ^{78}Kr , ^{80}Kr , ^{82}Kr , ^{83}Kr , and ^{84}Kr isotopic abundances of the gas targets were 56.5, 34.2, 6.9, 1.2, and 1.1% for the enriched ^{78}Kr , 7.1, 50.8, 38.8, 3.0, and 0.3% for the enriched ^{80}Kr , and 0.2, 15.1, 76.8, 7.7, and 0.2% for the enriched ^{82}Kr . Four lithium-drifted silicon detectors cooled to dry ice temperature were used. The over-all experimental energy resolution was about 30 keV.

III. ENERGY LEVELS AND Q -VALUE DETERMINATION

Figure 1 shows three typical $\text{Kr}(d,p)$ spectra, taken at a laboratory angle of 70° for each of the enriched targets. Identification of proton groups was based on careful comparisons of spectra from the different targets with respect to both energy and intensity ratios. Since ^{78}Kr was pres-

ent only as 7.1 and 0.2% contaminants in the ^{80}Kr and ^{82}Kr targets, respectively, states in ^{79}Kr did not appear in the ^{81}Kr and the ^{83}Kr spectra, except for the ground state in the ^{81}Kr spectrum and an unambiguous assignment of the observed proton groups as leading to states in ^{79}Kr , ^{81}Kr , or ^{83}Kr was nearly always possible.

The published values¹⁰ for the $^{78, 80, 82}\text{Kr}(d, p)^{79, 81, 83}\text{Kr}$ ground-state reaction Q values are 6.143 ± 0.011 , 5.603 ± 0.100 , and 5.243 ± 0.006 MeV, respectively. Using the above values of the $^{78}\text{Kr}(d, p)^{79}\text{Kr}$ and $^{82}\text{Kr}(d, p)^{83}\text{Kr}$ ground-state Q values, and the corresponding peak locations in the spectra together with the location of the deuteron elastic scattering peak, the Q values of the observed proton groups were obtained using a least-squares fitting code. Corrections were applied for the energy loss of the reaction particles in passing through the exit gas and Mylar walls using the tables of Williamson and Boujot.¹¹ The Q -value determinations for a given group were checked for consistency and averaged. The absolute uncertainty in the Q -value determination is believed to be ± 20 keV. The $^{80}\text{Kr}(d, p)^{81}\text{Kr}$ ground-state Q value could be determined with somewhat greater precision since this state had an energy between those of the $^{78}\text{Kr}(d, p)^{79}\text{Kr}$ and $^{82}\text{Kr}(d, p)^{83}\text{Kr}$ ground

states whose Q values are accurately known.¹⁰ We assign the $^{80}\text{Kr}(d, p)^{81}\text{Kr}$ ground-state Q value as 5.610 ± 0.015 MeV, in agreement with the published¹⁰ value of 5.630 ± 0.100 MeV. The ^{81}Kr mass excess was extracted from this measurement, with the relevant known mass excess values being taken from a recent mass compilation.¹² The (d, p) results led to a mass excess for ^{81}Kr of $-77\,659 \pm 15$ keV, consistent with the value of $-77\,680 \pm 100$ keV given in the mass tables. The Garvey-Kelson mass prediction¹³ yields a mass excess of $-77\,760$ keV for ^{81}Kr , in slight disagreement with the measured value.

IV. ANALYSIS OF ANGULAR DISTRIBUTIONS

The optical-model parameters needed to calculate the waves in the entrance and exit channels for the distorted-wave-Born-approximation (DWBA) calculations were obtained by fitting the appropriate proton and deuteron elastic scattering cross sections using a computer code written by Tamura and Bledsoe.¹⁴ These fits were carried out using the usual form for the optical potential with a surface absorption term and a real Thomas-type spin-orbit term.¹⁵ For the exit channel, optical parameters deduced from a fit to 12.0-MeV

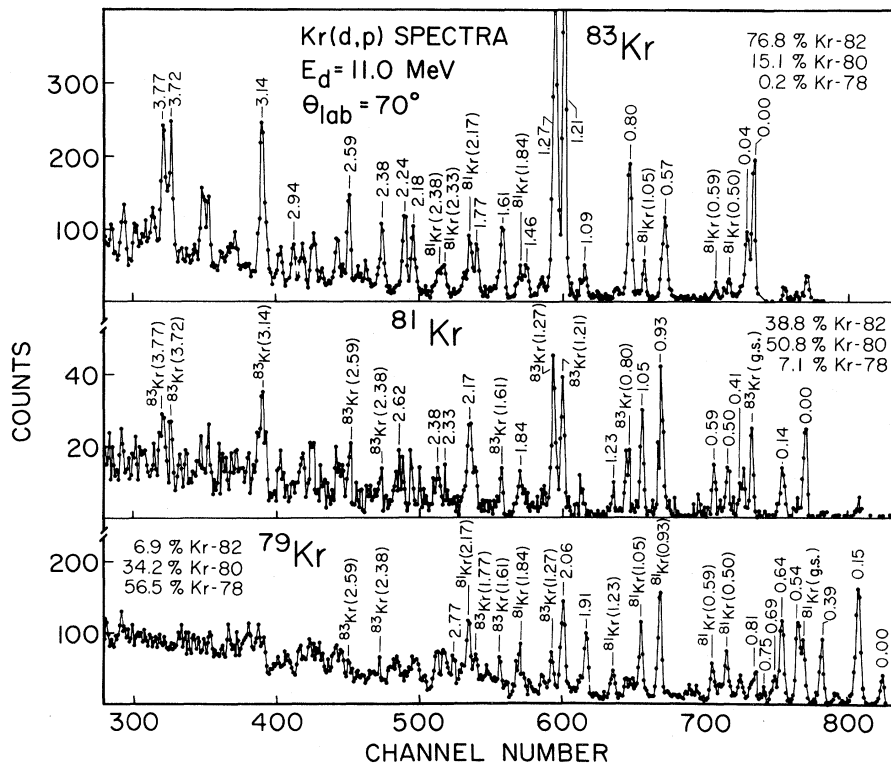


FIG. 1. Typical $\text{Kr}(d, p)$ spectra taken with identical energy scales for the three isotopically enriched krypton target gases used in the experiment.

proton scattering from natural krypton were used.⁶ These resulting proton optical parameters are as follows:

$$\begin{aligned} V &= 50.48 \text{ MeV}, & r_R &= 1.26 \text{ fm}, & a_R &= 0.65 \text{ fm}, \\ W_D &= 13.77 \text{ MeV}, & r_I &= 1.20 \text{ fm}, & a_I &= 0.53 \text{ fm}, \\ V_{so} &= 6.80 \text{ MeV}, & r_{so} &= 1.26 \text{ fm}, & a_{so} &= 0.72 \text{ fm}. \\ & & r_C &= 1.27 \text{ fm}, \end{aligned}$$

Because the outgoing energies of the various proton groups had a wide range, an energy dependent real well depth $V = (54.08 - 0.30E)$ MeV was employed for the DWBA fits. Figure 2 shows the experimental deuteron elastic cross section obtained from the ^{82}Kr enriched target, the best-fit optical-model parameters for the data, and the best fit. Almost identical parameters gave the best fit to the experimental elastic cross sections from the isotopically enriched ^{80}Kr and ^{78}Kr targets, and hence the parameters of Fig. 2 were used in all of the following DWBA analyses.

Differential cross sections for (d, p) transitions to 12 of the states in ^{83}Kr , 11 of the states in ^{81}Kr , and 10 of the states in ^{79}Kr which were sufficiently populated and resolved were fitted. The zero-

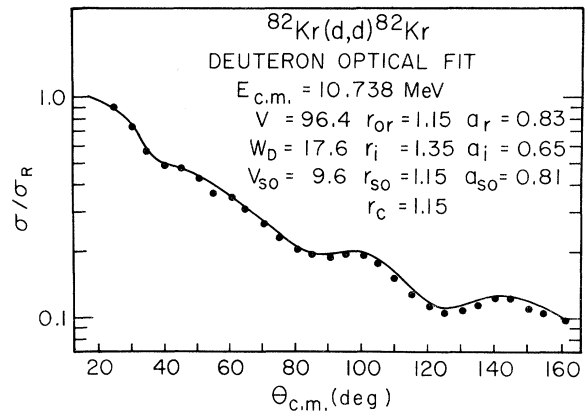


FIG. 2. Angular distribution of deuterons elastically scattered from the enriched ^{82}Kr gas target and the resulting optical-model fit. The best-fit optical-model parameters are as shown.

range DWBA computer code VENUS written by Tamura, Coker, and Rybicki¹⁶ with corrections for the nonlocality of the optical potential, was used. The bound-state neutron wave functions were calculated with the computer code NEPTUNE.¹⁶

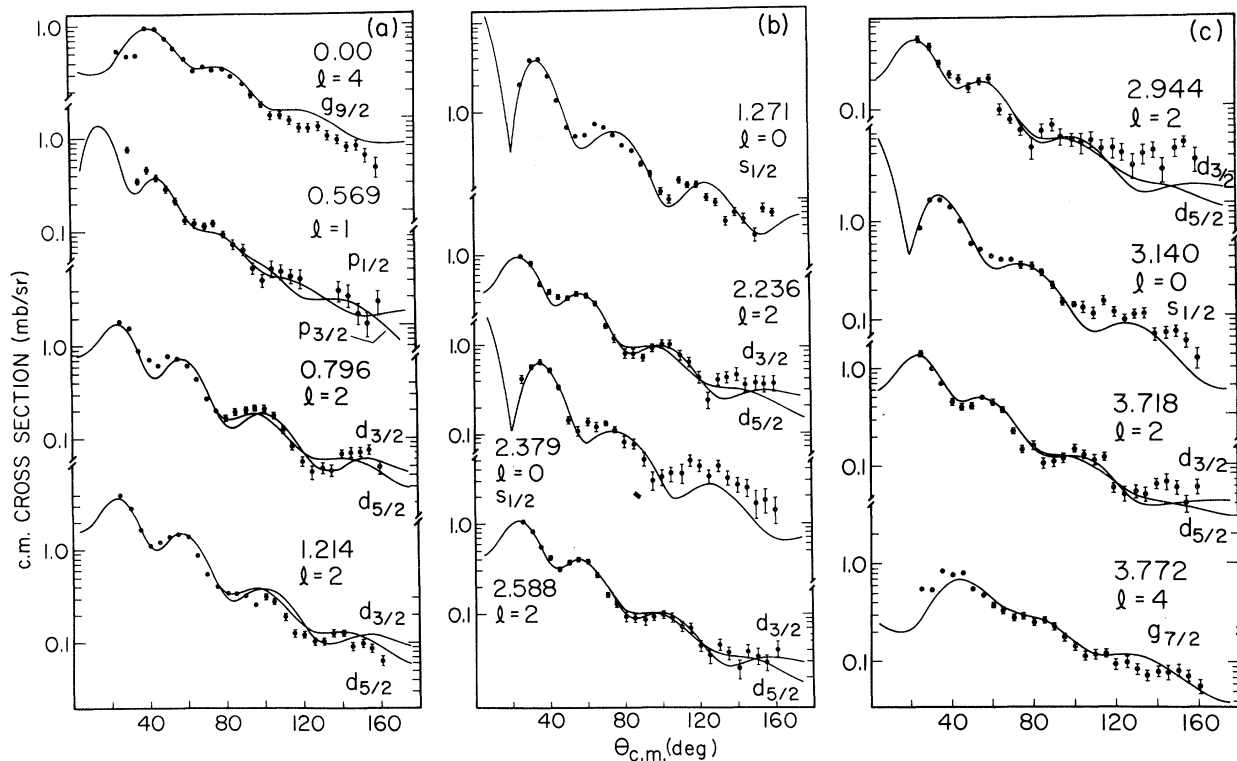


FIG. 3. (a)–(c) Angular distributions of $^{82}\text{Kr}(d, p)^{83}\text{Kr}$ transitions. The curves are DWBA fits to the experimental cross sections. Excitation energies and deduced l values are shown. The j^π values used to obtain the fits are indicated on the figure.

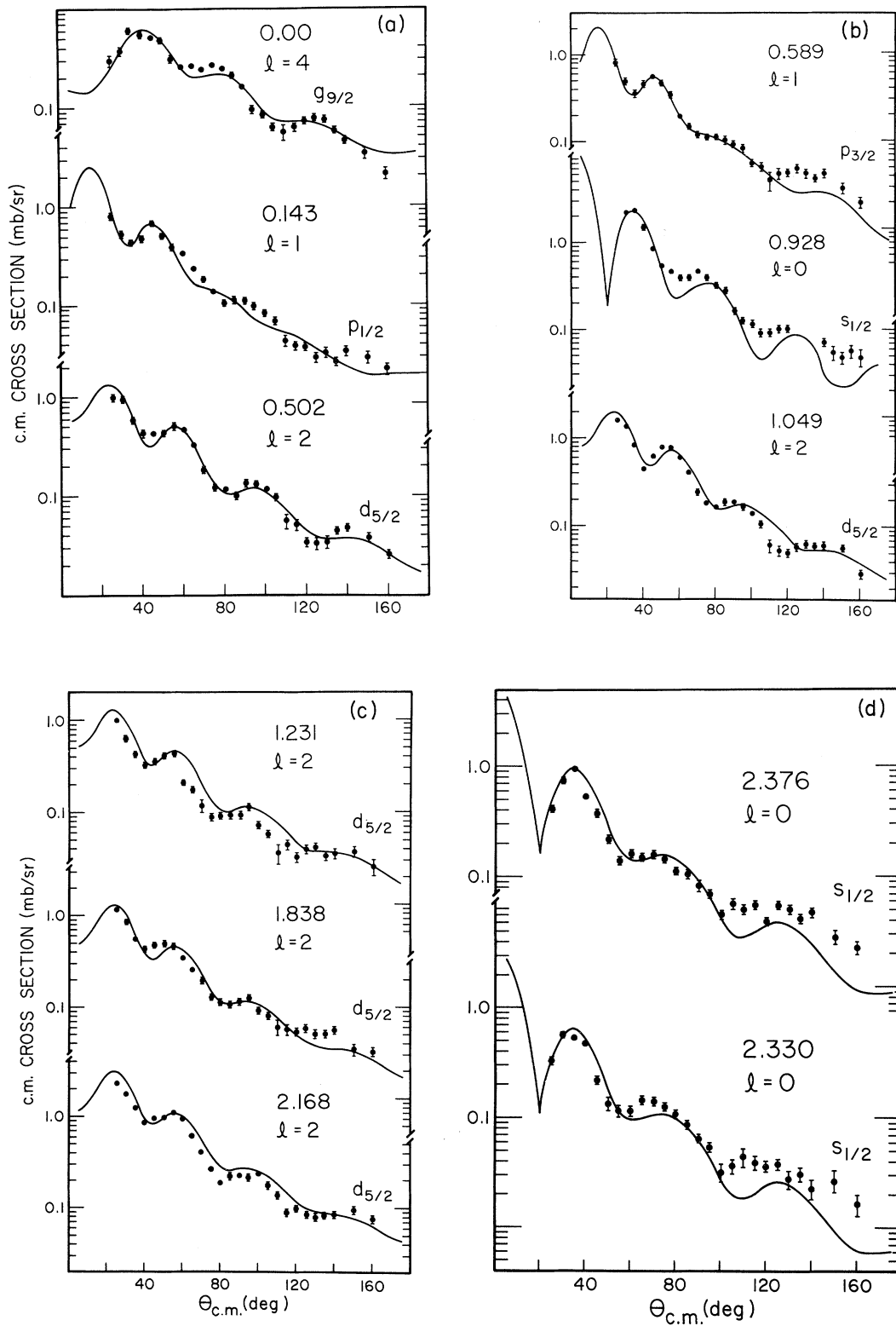


FIG. 4. (a)–(d) Angular distributions of $^{80}\text{Kr}(d,p)^{81}\text{Kr}$ transitions. The curves are DWBA fits to the experimental cross sections. Excitation energies and deduced l values are shown. The j^π values used to obtain the fits are indicated on the figure.

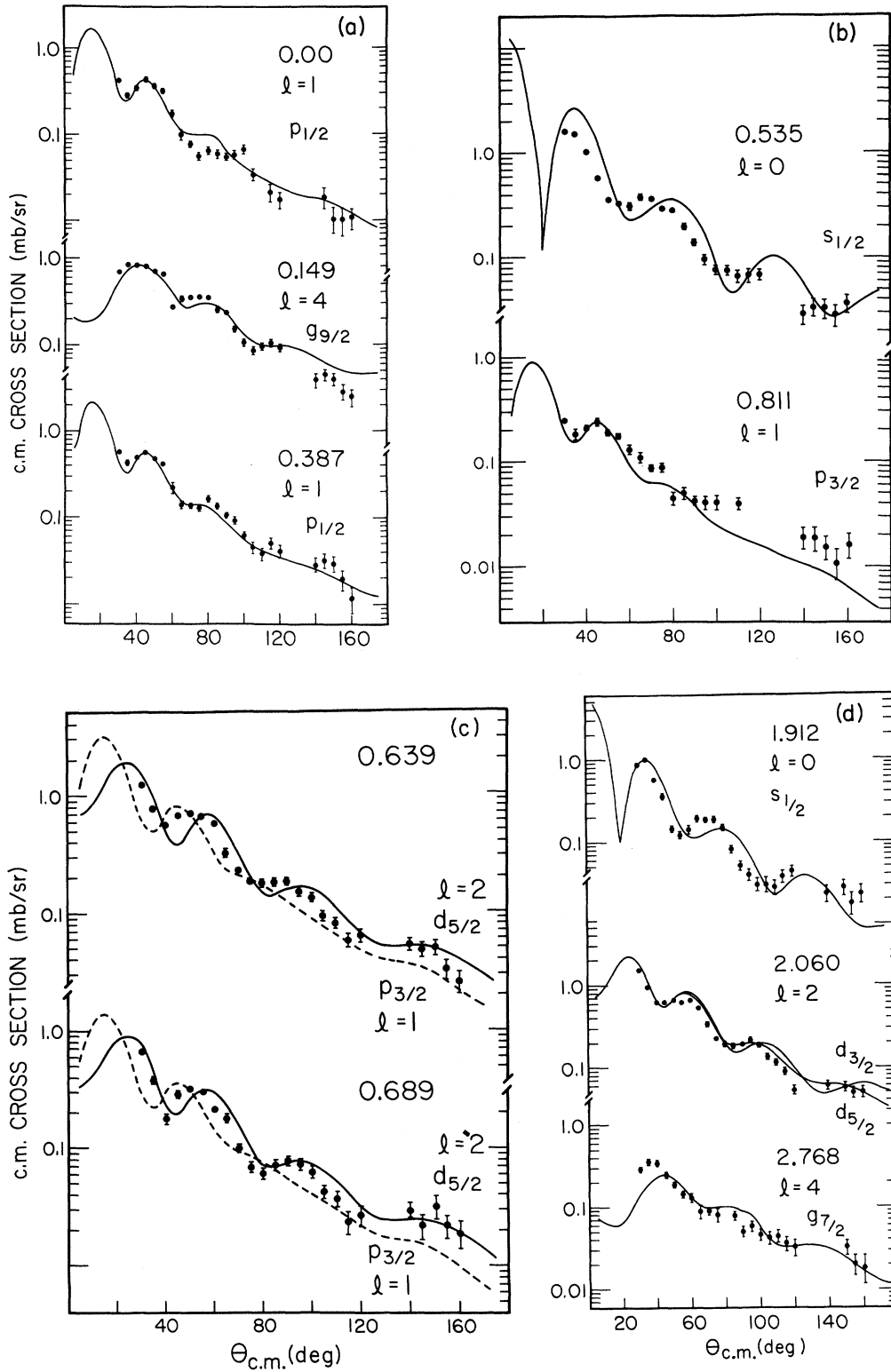


FIG. 5. (a)–(d) Angular distributions of $^{78}\text{Kr}(d, p)^{79}\text{Kr}$ transitions. The curves are DWBA fits to the experimental cross sections. Excitation energies and deduced l values are shown. The j^π values used to obtain the fits are indicated on the figure.

A Woods-Saxon well having essentially the same geometry as the real part of the proton optical potential was chosen for the form-factor calculation. A search for the Woods-Saxon well depth was made to reproduce the experimentally determined separation energy of each level.

The experimental cross sections to states in ^{83}Kr , ^{81}Kr , and ^{79}Kr are shown together with the DWBA fits in Figs. 3-5, respectively. In some cases difficulties were caused by overlapping peaks on the spectra from two different isotopes. For example, the 0.569-MeV state in ^{83}Kr could not be resolved from the 0.928-MeV state in ^{81}Kr . The cross section to the 0.928-MeV state in ^{81}Kr was therefore extracted from the spectra taken with the ^{78}Kr enriched target, in which ^{82}Kr was present only as a 6.9% contaminant. The contribution from the 0.928-MeV state in ^{81}Kr was then subtracted from the 0.569-MeV state in the spectra taken with the ^{82}Kr enriched target. As a consistency check, the cross sections for the two states, weighted by the appropriate isotopic abundances, were summed and shown to reproduce the cross section obtained from the ^{80}Kr enriched target gas for this doublet.

Over all, the agreement between the data and the DWBA predictions is reasonably good and we are confident of the l values deduced. However, improved experimental energy resolution and higher isotopic enrichments would be necessary to extract accurate cross sections to the more weakly populated states.

TABLE I. Energy levels of 79 , 81 , ^{83}Kr observed in the present work.

^{83}Kr (MeV)	^{81}Kr (MeV)	^{79}Kr (MeV)
0.00	0.00	0.00
0.035	0.143	0.149
0.569	0.414	0.387
0.796	0.502	0.535
1.085	0.589	0.639
1.214	0.928	0.689
1.271	1.049	0.749
1.460	1.231	0.811
1.614	1.838	1.912
1.773	2.168	2.060
2.183	2.330	2.768
2.236	2.376	
2.379	2.624	
2.588		
2.944		
3.140		
3.718		
3.772		

V. DISCUSSION

In the krypton region, the $2p_{3/2}$, $1f_{5/2}$, $2p_{1/2}$, and $1g_{9/2}$ orbits below the $N=50$ shell closure and the $2d_{5/2}$, $3s_{1/2}$, $2d_{3/2}$, and $1g_{7/2}$ orbits above the $N=50$ shell closure are expected to be populated by (d, p) transitions. Thus the spin-parity assignments for the levels populated by $l=0$ and 3 transfers are uniquely determined to be $\frac{1}{2}^+$ and $\frac{5}{2}^-$, respectively. The spin-orbit splitting of $1g_{9/2}$ and $1g_{7/2}$ states is expected to be at least 3 MeV, and therefore $1g_{7/2}$ states can be expected only at the highest excitation energies observed in the present work. There is therefore little ambiguity expected in distinguishing between $\frac{3}{2}^+$ and $\frac{7}{2}^+$ states for $l=4$ transfers. There remains the ambiguity in spin assignment for $l=1$ and 2 levels. In previous work on the germanium isotopes, Kato³ was able to distinguish two groups of levels populated by $l=1$ transitions, the energy separation between them being about 0.8 MeV. This energy separation was assumed to be due to the spin-orbit splitting between the $2p_{1/2}$ and $2p_{3/2}$ shell-model states; those states with the higher excitation energies were assigned to $2p_{3/2}$ and those with the lower energies assigned to $2p_{1/2}$. Although in the present work it is evident that some of the low-lying states could not be analyzed, the $l=1$ states do fall into two groups separated by about 600 keV of excitation energy. Again, the low-lying states are tentatively designated as $2p_{1/2}$, and the higher $l=1$ states as $2p_{3/2}$. There is no apparent j dependence either in the experimental data or in the DWBA fits for either $l=1$ or $l=2$ transitions. The $l=2$ strength in the krypton isotopes has been found to be rather fragmented, and spread over several MeV of excitation, with a larger spreading indicated for the lighter isotopes. The splitting between $2d_{5/2}$ and $2d_{3/2}$ states has been found to be about 3 MeV for nuclei near $A=100^3$. In the present work, we therefore expect to observe $2d_{3/2}$ states starting near 4.0 MeV of excitation, and probably $2d_{5/2}$ states are above the range of excitation observed in the present measurements. We therefore tentatively assign all the observed $l=2$ levels as $2d_{5/2}$ except for the 3.718-MeV state in ^{83}Kr .

The fits for ^{83}Kr shown in Fig. 3(a) indicate that the ground state, 0.569-, 0.796-, and 1.214-MeV states are, respectively, populated by $l=4$, 1, 2, and 2 transitions. From shell-model considerations, the ground state is expected to be $\frac{3}{2}^+$, whereas the two $l=2$ states are indicative of the filling of the $2d_{5/2}$ orbit above the $N=50$ shell closure. Two calculated curves are shown for the $l=2$ cross sections, one for $2d_{3/2}$ transitions and one for $2d_{5/2}$ transitions. Clearly from the

experimental cross sections one cannot choose between the two. Figures 3(b) and 3(c) show the experimental and calculated cross sections to the remaining states in ⁸³Kr that could be fitted. As expected from shell-model considerations, all of these states are fitted with *l*=0, 2, or 4 transfers. The weak states at excitation energies of 0.035, 1.085, 1.460, 1.614, 1.773, and 2.183 MeV in ⁸³Kr were either too poorly resolved to permit extraction of adequate angular distribution data, or could not be fitted by the DWBA. The 0.569-MeV state is the only *l*=1 transition observed in ⁸³Kr, allowing possible spin assignments of $\frac{1}{2}^-$ or $\frac{3}{2}^-$; a comparison with ⁷⁹Kr and ⁸¹Kr favors a tentative assignment of $\frac{3}{2}^-$ to this state. This would then indicate that the unresolved 0.035-MeV state is probably the missing $\frac{1}{2}^-$ state in ⁸³Kr. The weak states between 1.0- and 2.0-MeV excitation which have not been fitted are then most probably *l*=0 or 2 transitions.

The experimental and calculated cross sections to ⁸¹Kr are shown in Figs. 4(a)–4(c). The ground state is still fitted with a $\frac{9}{2}^+$ assignment; however, a strong *l*=1 ($\frac{1}{2}^-$) state appears at 0.143 MeV. The 0.502-MeV state is fitted with *l*=2 transition; consistent with a $\frac{5}{2}^+$ assignment, whereas the 0.589-MeV state is fitted with *l*=1 transition indicative of a $\frac{3}{2}^-$ (or $\frac{1}{2}^-$) assignment. The remaining states analyzed above the 0.589-MeV state are all fitted with either *l*=0 or 2 transfers.

For transitions to ⁷⁹Kr, as shown in Figs. 5(a)–5(c), the ground state is fitted with a *l*=1 transition ($\frac{1}{2}^-$), and first excited state at 0.149 MeV of

excitation with an *l*=4 transfer ($\frac{9}{2}^+$). Again, there is apparent overlapping of $\frac{3}{2}^-$ strength (0.811 MeV) with $\frac{1}{2}^+$ (0.535 MeV) and $\frac{5}{2}^+$ (0.639 and 0.689 MeV) states above the *N*=50 shell closure. An increase in fractionation of the single-particle strength in the krypton isotopes furthest away from the closed *N*=50 shell is evident.

The nucleus ⁷⁹Kr has been previously studied via ⁷⁹Rb decay measurements.^{8,9} The present (*d, p*) work is in agreement with the assignment of $\frac{1}{2}^-$ for the ground state of ⁷⁹Kr. The excited states seen in our (*d, p*) measurements at 149 (*l*=4), 387 (*l*=1), 535, 689 (*l*=2), and 749 keV of excitation apparently correspond to states in the decay work^{8,9} at excitations of 147, 384, 533, 688, and 752 keV, with respective spin assignments of $\frac{5}{2}^-$, $-$, ($\frac{1}{2}^-$, $\frac{3}{2}^-$, $\frac{5}{2}^-$), ($\frac{1}{2}^-$, $\frac{3}{2}^-$), and $\frac{5}{2}^-$. Unfortunately, there appear to be two very real discrepancies between the two sets of measurements. The half-life and γ -decay intensities to the ground state and 130-keV state are consistent *only* with a $\frac{3}{2}^-$ spin assignment for the 147-keV state. A $\frac{5}{2}^-$ assignment would imply an *l*=3 assignment for the (*d, p*) work. However, the DWBA analysis clearly indicates an *l*=4 transition. The second problem occurs with the 689-keV level, deduced to be $\frac{1}{2}^-$ or $\frac{3}{2}^-$ in the decay work. Our experiment gives *l*=2 for this state. However, the *l*=2 DWBA fits to this state and to the 639-keV state are not good, and *l*=1 fits are also shown in Fig. 5(b). It is possible that the 689-keV level, which is not clearly resolved from the large 639-keV level, could be fitted with *l*=1 transfer, even

TABLE II. Summary of DWBA analysis of the states of ⁸³Kr via the reaction ⁸²Kr(*d, p*)⁸³Kr.

<i>E</i> [*] (MeV)	<i>l</i> _{<i>n</i>}	<i>J</i> ^π	<i>dσ/dΩ</i> (max) (mb/sr)	<i>S</i> _{<i>J</i>}
0.00	4	$\frac{9}{2}^+$	0.941	0.458
0.569	1	($\frac{3}{2}^-$)	0.784	0.084
0.796	2	$\frac{5}{2}^+$	1.861	0.146
1.214	2	$\frac{5}{2}^+$	3.988	0.283
1.271	0	$\frac{1}{2}^+$	4.009	0.336
2.236	2	$\frac{5}{2}^+$	1.027	0.0581
2.379	0	$\frac{1}{2}^+$	0.637	0.0487
2.588	2	($\frac{5}{2}^+$)	1.028	0.0601
2.944	2	($\frac{5}{2}^+$)	0.520	0.0268
3.140	0	$\frac{1}{2}^+$	1.624	0.139
3.718	2	($\frac{3}{2}^+$)	1.389	0.0830
3.772	4	$\frac{7}{2}^+$	0.835	0.356

TABLE III. Summary of the DWBA analysis of the states of ⁸¹Kr via the reaction ⁸⁰Kr(*d, p*)⁸¹Kr.

<i>E</i> [*] (MeV)	<i>l</i> _{<i>n</i>}	<i>J</i> ^π	<i>dσ/dΩ</i> (max) (mb/sr)	<i>S</i> _{<i>J</i>}
0.0	4	$\frac{9}{2}^+$	0.605	0.376
0.143	1	$\frac{1}{2}^-$	0.816	0.423
0.414				
0.502	2	$\frac{5}{2}^+$	0.978	0.122
0.589	1	($\frac{3}{2}^-$)	0.807	0.145
0.928	0	$\frac{1}{2}^+$	2.285	0.253
1.049	2	$\frac{5}{2}^+$	1.590	0.162
1.231	2	$\frac{5}{2}^+$	0.995	0.104
1.838	2	$\frac{5}{2}^+$	1.187	0.093
2.168	2	$\frac{5}{2}^+$	2.270	0.207
2.330	0	$\frac{1}{2}^+$	0.561	0.060
2.376	0	$\frac{1}{2}^+$	0.951	0.089
2.624				

though this does not appear likely.

Tables II-IV summarize the results of the DWBA analyses for ^{83}Kr , ^{81}Kr , and ^{79}Kr , respectively. The last column of the table give the spectroscopic factor S_J , defined as

$$S_J = \sigma_{\text{exp}} / [(2J+1)\sigma_{\text{DWBA}}] . \quad (1)$$

Except possibly for the 639- and 689-keV states in ^{79}Kr , we believe the l assignments to be unique; the J^π assignments have been discussed above. The more tentative spin assignments are given in parentheses; however, in the absence of polarization data, the spin assignments for nonzero l transfers must not be considered definitive even where parentheses are not shown.

Figure 6 shows an energy-level diagram for the krypton isotopes. The length of the lines is proportional to the spectroscopic factors. The ^{85}Kr levels are taken from the work of Browne *et al.*,⁶ and those for ^{87}Kr from the measurements of Haravu *et al.*⁷ The energy levels for ^{87}Kr have been displaced upwards by 1 MeV so that the strong ^{87}Kr $2d_{5/2}$ ground state is approximately aligned with the strong low-lying $2d_{5/2}$ states in the lighter krypton isotopes. A general increase in fractionation of the $2d_{5/2}$ and $3s_{1/2}$ strengths is evident for the lighter krypton isotopes, and it is probable that not all of the $2d_{5/2}$ and $3s_{1/2}$ states have been identified in the present work. Clearly, most of the $2d_{3/2}$ and $1g_{7/2}$ strength lies above the region of excitation observed in the present work, although a relatively strong $1g_{7/2}$ state is identified in ^{83}Kr . An increase in strength of the low-lying $2p_{1/2}$, $2p_{3/2}$, and $1g_{9/2}$ states is also evident

TABLE IV. Summary of the DWBA analysis of the states of ^{79}Kr via the reaction $^{78}\text{Kr}(d,p)^{79}\text{Kr}$.

E^* (MeV)	l_n	J^π	$d\sigma/d\Omega$ (max) (mb/sr)	S_J
0.000	1	$\frac{1}{2}^-$	0.428	0.305
0.149	4	$\frac{9}{2}^+$	0.858	0.512
0.387	1	$(\frac{1}{2}^-)$	0.581	0.366
0.535	0	$\frac{1}{2}^+$	1.582	0.341
0.639	2	$\frac{5}{2}^+$	1.221	0.174
0.689	(2)	$(\frac{5}{2}^+)$	0.661	0.0808
0.749				
0.811	1	$\frac{3}{2}^-$	0.239	0.064
1.912	0	$\frac{1}{2}^+$	1.016	0.104
2.060	2	$(\frac{5}{2}^+)$	1.548	0.162
2.768	4	$\frac{7}{2}^+$	0.355	0.176

for the lighter krypton isotopes. No $l=3$ ($1f_{5/2}$) states were identified, indicating that the $1f_{5/2}$ subshell must be rather full in the stable krypton isotopes. The excitation energy of the first $2p_{1/2}$ state decreases for the lighter krypton isotopes, until for ^{79}Kr the ground state is $\frac{1}{2}^-$.

The krypton isotopes have recently been studied by means of γ -ray spectroscopy methods in Se + α reactions.¹⁷ These investigations suggest that there are low-lying rotational bands in ^{77}Kr , ^{79}Kr , and ^{81}Kr . Specifically, low-lying $\frac{1}{2}^-$ and $\frac{5}{2}^-$ states have been found which should have a pronounced hole character. These states are

$$^{79}\text{Kr}: 147 \text{ keV } (\frac{5}{2}^-) \text{ and } 183 \text{ keV } (\frac{1}{2}^-),$$

$$^{81}\text{Kr}: 190 \text{ keV } (\frac{1}{2}^-) \text{ and } 549 \text{ keV } (\frac{5}{2}^-).$$

Of these, only a 149-keV state is seen in ^{79}Kr in the present work; as discussed previously, this state is fitted well by $l=4$ transition, indicating a $\frac{9}{2}^+$ rather than a $\frac{5}{2}^-$ assignment. It is clear that higher resolution measurements with better isotopic enrichments will be necessary to resolve the apparent discrepancies; both with the above work and with decay measurements.

To study the gross structure of the shell-model states, a sum-rule analysis was applied to the present experimental results. The summed spectroscopic factor $\sum_i S_i^J$ represents the vacancy of the shell-model state in a doubly even target nucleus. Another important set of numbers are the spectroscopic-factor-weighted energy centroids E_J . These centroids are defined by the equation

$$\bar{E}_J = \frac{\sum_i E_i S_i^J}{\sum_i S_i^J} . \quad (2)$$

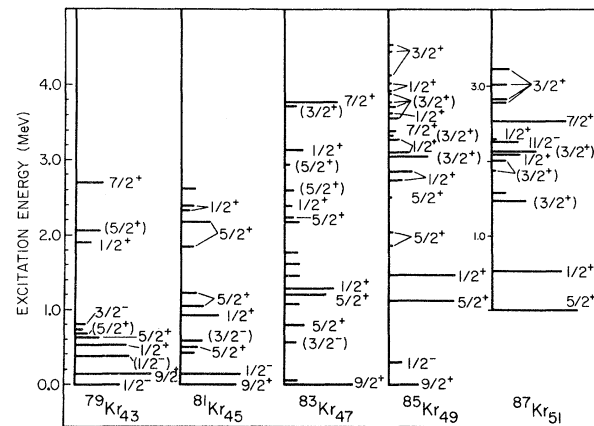


FIG. 6. Energy level diagrams deduced from $\text{Kr}(d,p)$ measurements on the even krypton isotopes. The length of the lines is proportional to the spectroscopic factors. The ^{85}Kr levels are taken from Ref. 6 and those for ^{87}Kr from Ref. 7.

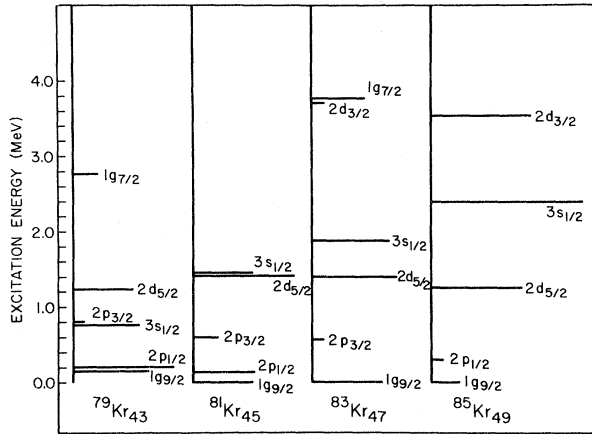


FIG. 7. The sums of the spectroscopic factors and the centroid energies for the krypton isotopes. The lengths of the horizontal lines are proportional to the sums of the spectroscopic factors.

The sums of the spectroscopic factors and the centroid energies for the krypton isotopes are shown plotted in Fig. 7, and are listed in Table V. The length of the horizontal lines is proportional to the sums of the appropriate spectroscopic factors. The 0.035-MeV transition in ⁸³Kr is a likely candidate for a *p*_{1/2} state, and the four weak states between 1.0 and 2.0 MeV excitation are then most probably *l*=0 or 2 transitions. This would have the effect of slightly increasing the values $\sum_i S_i^{1/2}$ and/or $\sum_i S_i^{5/2}$ for ⁸³Kr in Table V.

For shell-model orbitals above *N*=50, the centroid energy for 3*s*_{1/2} states increases uniformly from 0.76 MeV to ⁷⁹Kr to 2.39 MeV for ⁸⁵Kr, whereas the 2*d*_{5/2} centroid energy remains rather constant at about 1.4 MeV. For the 2*p*_{3/2}, 2*p*_{1/2}, and 1*g*_{9/2} orbitals below *N*=50, the number of neutrons calculated to be outside the *N*=28 closed

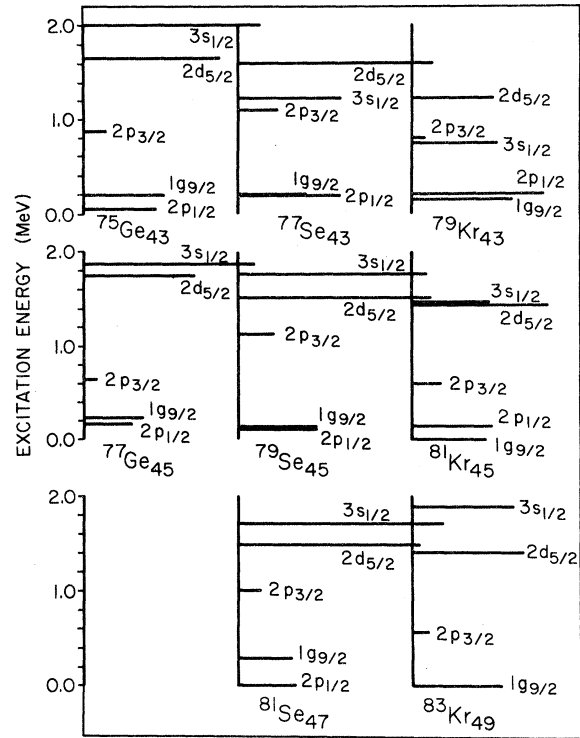


FIG. 8. A comparison of the summed spectroscopic factors and the centroid energies for the krypton isotopes, obtained in the present work, and those deduced for the germanium (Ref. 3) and selenium (Ref. 4) isotopes. Comparisons are made between nuclei with the same number of neutrons. The lengths of the horizontal lines are proportional to the sums of the spectroscopic factors.

shell from the equation¹⁸

$$n = \sum_J (2J+1) \left(1 - \sum S_J\right) \quad (3)$$

is in reasonable agreement with the expected num-

TABLE V. Sums of the spectroscopic factors and the centroid energies for the krypton isotopes as found in the present work for the indicated shell-model orbits. Comparisons based on pairing theory are shown for the 2*p*_{3/2}, 2*p*_{1/2}, and 1*g*_{9/2} orbitals.

		Shell-model orbits							
		2 <i>p</i> _{3/2}		2 <i>p</i> _{1/2}		1 <i>g</i> _{9/2}		2 <i>d</i> _{5/2}	3 <i>s</i> _{1/2}
		Exptl.	Theory ^a	Exptl.	Theory ^a	Exptl.	Theory ^a		
$\sum_i S_i^f$	⁷⁹ Kr	0.06	0.03	0.67	0.21	0.51	0.64	0.42	0.44
	⁸¹ Kr	0.15	0.02	0.42	0.12	0.38	0.46	0.69	0.40
	⁸³ Kr	0.08	0.02	•••	0.06	0.46	0.28	0.57	0.52
	⁸⁵ Kr ^b	•••	0.00	0.08	0.00	0.19	0.50	0.62	1.03
\bar{E}_J (MeV)	⁷⁹ Kr	0.81	2.09	0.21	0.00	0.15	-0.22	1.23	0.76
	⁸¹ Kr	0.59	2.79	0.14	0.58	0.00	0.00	1.42	1.46
	⁸³ Kr	0.57	3.21	•••	0.91	0.00	0.00	1.40	1.88
	⁸⁵ Kr ^b			0.30	1.26	0.00	0.00	0.26	2.39

^a Based on parameters of Ref. 19.

^b Reference 6.

ber. In Table V a comparison has been made for the $2p_{3/2}$, $2p_{1/2}$, and $1g_{9/2}$ orbitals between the experimental results and the values U_j^2 for the non-occupation probabilities, and the quasiparticle energies E_j , deduced from pairing theory.¹⁹ The values of ϵ_j and Δ have been taken from Ref. 19. It is evident that for the $2p_{3/2}$ and $2p_{1/2}$ subshells the experimental values of $\sum S$ are much larger than the corresponding predicted values of U_j^2 , and the experimental values of E_j are lower than the predicted values. It is probable that for these nuclei such effects as the proton-neutron interaction and the long-range quadrupole interaction, ignored in the simple pairing theory, may be rather important. Rather similar results were obtained by Lin⁴ in attempting to explain (d, p) and (d, t) data on the Se isotopes in terms of pairing theory.

The summed spectroscopic energies and centroid energies of the present work in the krypton isotopes are compared with corresponding results,

obtained in studies of germanium and selenium isotopes in Fig. 8. Again, the lengths of the horizontal lines are proportional to the sums of the spectroscopic factors. Comparisons are specifically made between nuclei with the same number of neutrons. For the 43-neutron nuclei ^{75}Ge , ^{77}Se , and ^{79}Kr there is a pronounced decrease in the centroid energies of $3s_{1/2}$ states between ^{75}Ge and ^{79}Kr . For the 45-neutron nuclei ^{77}Ge , ^{79}Se , and ^{81}Kr , and the 47-neutron nuclei ^{81}Se - ^{83}Kr , the centroid energies of the $3s_{1/2}$ and $2d_{5/2}$ states are about constant. The $2p_{3/2}$ centroid energies appear consistently higher in the selenium isotopes than in either of the germanium or krypton isotopes. The $1g_{9/2}$ and $2p_{1/2}$ centroid energies are in reasonable agreement for all isotopes.

The authors gratefully acknowledge the assistance of B. K. Arora, C. Chang, and W. Craig with the data taking. Thanks are due W. R. Coker for helpful discussions.

*Work supported in part by the U.S. Atomic Energy Commission.

† Present address: Oak Ridge National Laboratory, P. O. Box X, Oak Ridge, Tennessee, 37830.

¹R. H. Fulmer, A. L. McCarthy, B. L. Cohen, and R. Middleton, *Phys. Rev.* **133**, B955 (1964).

²D. von Ehrenstein and J. P. Schiffer, *Phys. Rev.* **164**, 1374 (1967).

³N. Kato, *Nucl. Phys.* **A203**, 97 (1973).

⁴E. K. Lin, *Phys. Rev.* **139**, B340 (1965).

⁵J. Chao, B. K. Arora, C. Chang, W. Craig, C. Newsom, D. K. Olsen, and P. J. Riley, *Bull. Am. Phys. Soc.* **19**, 450 (1974).

⁶C. P. Browne, D. K. Olsen, J. Chao, and P. J. Riley, *Phys. Rev. C* **9**, 1831 (1974).

⁷K. Haravu, C. L. Hollas, P. J. Riley, and W. R. Coker, *Phys. Rev. C* **1**, 938 (1970).

⁸E. W. A. Lingeman, F. W. H. De Boer, P. Koldewijn, and P. R. Maurenzig, *Nucl. Phys.* **A160**, 630 (1971).

⁹R. Broda, M. Rybicka, J. Styczen, W. Walus, and K. Krolas, *Acta. Phys. Pol. B* **3**, 263 (1972).

¹⁰N. B. Gove and A. H. Wapstra, *Nucl. Data* **A11**, 177 (1972).

¹¹C. Williamson and J. P. Boujot, Centre d'Etudes Nucleaires de Saclay Report, 1962 (unpublished).

¹²A. H. Wapstra and N. B. Gove, *Nucl. Data* **A9**, 265 (1971).

¹³G. T. Garvey and I. Kelson, *Phys. Rev. Lett.* **16**, 197 (1966); G. T. Garvey, W. J. Gerace, R. L. Jaffe, I. Talmi, and I. Kelson, *Rev. Mod. Phys.* **41**, 51 (1969).

¹⁴T. Tamura and H. Bledsoe, private communication.

¹⁵S. Sen, C. L. Hollas, C. W. Bjork, and P. J. Riley, *Phys. Rev. C* **5**, 1278 (1972).

¹⁶T. Tamura, W. R. Coker, and F. Rybicki, *Comput. Phys. Commun.* **2**, 94 (1971).

¹⁷A. P. Sawa, Research Institute for Physics, Stockholm, Sweden, private communication.

¹⁸L. H. Goldman, *Phys. Rev.* **165**, 1203 (1968).

¹⁹L. S. Kisslinger and R. A. Sorenson, *Rev. Mod. Phys.* **35**, 853 (1963).